Graphene synthesis on SiO2 using pulsed laser deposition with bilayer predominance

Yannick Bleu, Florent Bourquard, Valentin Gartiser, Anne-Sophie Loir, Borja Caja-Munoz, José Avila, Vincent Barnier, Florence Garrelie, Christophe Donnet

Graphene synthesis on SiO_2 using pulsed laser deposition with bilayer predominance

Yannick Bleu[1], Florent Bourquard[1], Valentin Gartiser[1], Anne-Sophie Loir[1], B. Caja-Munoz[3], J. Avila[3], Vincent Barnier[2], Florence Garrelie[1], and Christophe Donnet[1]

(1) Université de Lyon, Université Jean Monnet-Saint-Etienne, CNRS, Institut d'Optique Graduate School, Laboratoire Hubert Curien UMR 5516, F-42023, SAINT-ETIENNE, France
(2) Université de Lyon, Mines Saint-Etienne, CNRS, Laboratoire Georges Friedel UMR 5307 CNRS, F-42023 Saint-Etienne, France
(3) Synchrotron SOLEIL & Université Paris-Saclay, Saint Aubin, F-91192 Gif sur Yvette, France

Abstract

Here we report the low-defect synthesis of bilayer graphene film on SiO_2 with a nickel catalyst using pulsed laser deposition combined with rapid thermal annealing. A parametric study was performed with various initial amorphous carbon (a-C) film thicknesses and annealing temperatures and a fixed nickel catalyst film thickness. Raman spectra and mapping over large areas of up to 100 × 100 μm² were used to investigate the structure and the defects of graphene films. Optimal conditions for graphene growth were an initial a-C film thickness of 2 nm and an annealing temperature of 900°C. Results showed that 76% of the optimized film contained graphene bilayers, and 18% of the optimized film contained graphene monolayers. A transmittance of 87% at 550 nm is observed without any transfer process from the SiO_2 substrate. This paper presents experimental guidelines for optimal synthesis conditions to control graphene growth by pulsed laser deposition.

Keywords: Bilayer graphene, Pulsed laser deposition, Raman mapping

1. Introduction

Research on graphene has received considerable attention due to its outstanding physical and chemical properties, and its potential for a wide range of applications[1–5]. Several methods including mechanical exfoliation, annealing of SiC under ultrahigh vacuum, chemical vapor deposition (CVD), reduction of graphene oxide, and pulsed laser deposition (PLD) have been used to make graphene films[6–10]. Among these methods, PLD is one of the alternative physical routes to the commonly used CVD process. Originally, PLD was mainly used to deposit thin films with high crystallinity, accurate stoichiometry, and thickness controlled up to the atomic monolayer[11]. PLD has also been widely used for amorphous diamond-like carbon (DLC) synthesis, with different Csp^2/Csp^3 ratios[12]. In the present study, graphene films were synthesized using an amorphous solid carbon (DLC, or a-C) precursor with precisely controlled thickness. In the present study, graphene films were synthesized using an amorphous solid carbon (DLC, or a-C) precursor with precisely controlled thickness. From our best of knowledge, the presence of a metal catalyst is necessary for graphene synthesis from a solid carbon source. The absence of catalyst was previously investigated with CVD processes, in particular by Liu et al[13] and Barbosa et al.[14]. However, such a route appears to favor a significant density of defects, compared to synthesis routes using a metal catalyst. So, in the present study, we use a metal catalyst to obtain graphene layers with a low defect concentration. Several catalysts including nickel, copper, cobalt, copper-nickel alloy catalyst[15–20] have been used to obtain graphene from the carbon film precursor. Several studies have reported the growth of graphene by PLD using nickel catalyst[21–26]. In fact, graphene synthesis with nickel is due to segregation of carbon at high temperatures. Due to the high solubility of carbon in nickel, the carbon atoms diffuse through the nickel catalyst and precipitate on the surface during cooling[27,28]. As precipitation is a non-equilibrium process, controlling the thickness of the graphene is challenging[29–31]. In addition, most of the graphene films made by PLD using a nickel catalyst have turned out to be heterogeneous with a mixture of single and multilayered graphene sheets. There is thus a need to optimize the PLD process for graphene growth to obtain a uniform large-area monolayer or bilayer graphene. In the present work, we studied the influence of two process parameters, initial amorphous carbon (a-C) thickness and the annealing temperature, on the growth of graphene using PLD and rapid thermal annealing. Our parametric study identified the optimal conditions for growing predominantly bilayer graphene. The structure and defects of the graphene films were characterized using a micro-Raman spectroscopic technique. Raman

mapping was used for large areas of up to 100 × 100 μm² which has rarely been investigated but is indispensable to check lateral homogeneity, and statistical analysis to determine the number of layers and overall distribution of the graphene films on the substrate.

2. Experimental details

The different steps of sample preparation are shown in **Figure 1**. SiO_2 substrates were ultrasonically cleaned first in acetone, and then in ethanol and finally in deionized water baths. Nickel film (50 nm thick) was deposited by thermal evaporation on the top of the cleaned SiO_2 substrates in a vacuum chamber pumped at a base pressure of 10^{-6} mbar. High purity (99.99%) Ni was molten thermally in a tungsten nacelle and evaporated towards the substrate. The Ni/SiO_2 substrates were then placed in a vacuum PLD chamber pumped at a base pressure of 10^{-7} mbar for amorphous carbon (a-C) deposition. Carbon was ablated from high purity graphite (99.9995%) target using an excimer KrF laser (248 nm wavelength, 20 ns pulse duration, 10 Hz repetition rate) at room temperature. The fluence of the laser beam was kept constant at 5 $J.cm^{-2}$. The ablation time was adjusted to vary the thickness of the amorphous (a-C) film to 1, 2, 4, 5, 10 and 20 nm. Assuming a density of 3 $g.cm^{-3}$ for the deposited a-C films, this corresponds to a carbon flux of $3.8x10^{15}$ $C.cm^{-2}.s^{-1}$. The Ni/SiO_2 substrates were mounted on a sample holder placed at a distance of 40 mm from the graphite target. The final step consisted in heating the $a\text{-}C/Ni/SiO_2$ samples at temperatures ranging from 800 to 1000 °C for 420 s in a vacuum pressure of 10^{-2} mbar using a RTA oven, with a heating rate of +15 °C/s and a cooling rate of about -0.5°C/s. **Table 1** summarizes the processing conditions of the samples.

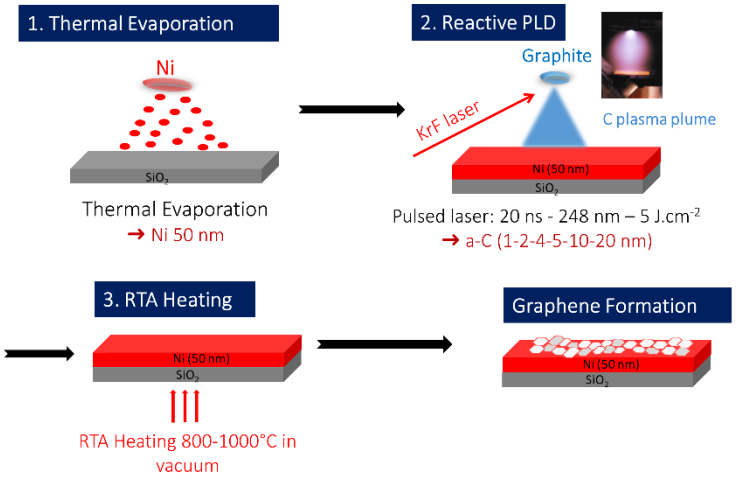

Figure 1: Synthesis route for graphene films obtained by pulsed laser deposition and rapid thermal annealing on SiO_2.

Raman spectroscopy was used to characterize the synthesized material with an Aramis Jobin Yvon spectrometer (Horiba Jobin Yvon, Gières, France), with 442 nm (2.81 eV) excitation laser focused through an x100 objective with a high aperture, guaranteeing the micrometric resolution of the analysis, and providing precise Raman maps of the samples. The laser power was kept below 3 mW to avoid damaging the surface of the film and the diameter of the laser beam was estimated to be near 1 micrometer, near the diffraction limit at this wavelength. To examine the uniformity of the synthesized graphene, mapping of probed surfaces 20 × 20 micrometers in size, was performed for all samples at 442 nm, totaling 400 Raman spectra per map with a 1 µm spot collected on each sample. For the sample with the optimal conditions, mapping was done in two different regions over areas of 20 x 20 µm² and 100 x100 µm². The Raman signals were acquired with a spectrometer equipped with a charge-coupled device (CCD) camera. Atomic Force microscopy measurements were performed using AGILENT 5500 microscope operating in tapping mode in the ambient environment at room temperature. All the images were obtained at 1 Hz, 512 x 512 pixels (image definition). The AFM image treatment and root mean square roughness (RMS) were determined with Gwyddion software. Scanning electron microscopy (SEM) images were recorded using a FEI Novanano SEM 200 operated at 15kV. XPS analysis was performed at Synchrotron SOLEIL (Saclay, France), ANTARES beam line. The ring operating conditions were 2.5 GeV electron energy, with injection currents of 500 mA and "Top-up" mode. Radiation was monochromatized using a plane-grating monochromator (PGM), which is characterized by a slitless entrance and the use

of two varied linear spacing (VLS) gratings with variable groove depth (VGD) along the grating lines. The diameter of the X-ray spot impinging the surface is 140 µm and the X-ray energy was fixed at 700 eV for analysis of the graphene film. The photoemission spectra were taken with incident photon energies of 700 eV (see details in each figure 9 panel), with 190 meV energy resolution. UV-Visible spectroscopy in transmission mode was performed by a spectrophotometer Cary50 Probe (Varian) within the spectral range 200-800 nm.

Ni catalyst thickness (nm)	a-C initial thickness (nm)	Rapid thermal annealing conditions
50	1	Temperature: 800-900-1000 °C Heating ramp: +15 °C/s Time: 420 s Cooling ramp: -0.5 °C/s
	2	
	4	
	5	
	10	
	20	

Table 1: Summary of the growth conditions.

3. Results

The initial a-C thickness and growth temperature play a major role in determining the number of layers and the quality of graphene grown on SiO_2 with a nickel catalyst. In order to investigate their effect on graphene film architecture, we considered 18 sets of graphene growth conditions, crossing 6 initial a-C thicknesses with 3 annealing temperatures. All samples were characterized by Raman spectroscopy and mapping, the most widely used technique to investigate the structure, defects, and the number of layers in graphene materials[32–34]. In graphene films, the D, G, and 2D bands are the most significant features observed in Raman spectroscopy. The G band appears near 1 580 cm^{-1} and is associated with covalent C–C bonding vibrations in the graphite matrix and is present in every carbon

material containing sp^2 bonding. The D band is located around 1 350 cm^{-1}, is associated with the pulsation of aromatic circles and appears only in the presence of defects and dislocations in the graphitic matrix. The intensity ratio between the D band and G band (I_D/I_G) is thus an indication of disorder in the graphene structure. The 2D band is situated around 2 700 cm^{-1} and is associated with a double resonance Raman scattering process. For graphene and graphite materials, the intensity ratio of the 2D band versus the G band (I_{2D}/I_G) is a good indicator to identify the number of graphene layers. It is generally accepted that an I_{2D}/I_G ratio >1.4 represents the formation of monolayer graphene. Bilayer graphene can be identified with a I_{2D}/I_G ratio of between 0.75 and 1.4, and graphene with three and more layers can be identified with a I_{2D}/I_G ratio < 0.75[35–37].

3.1. Graphene layer number distribution through I_{2D}/I_G ratio mapping, as a function of the initial thickness of a-C and annealing temperature

Figures 2 and 3 show the Raman maps and the average values of the I_{2D}/I_G ratio of all the samples over an area of 20 x 20 µm².

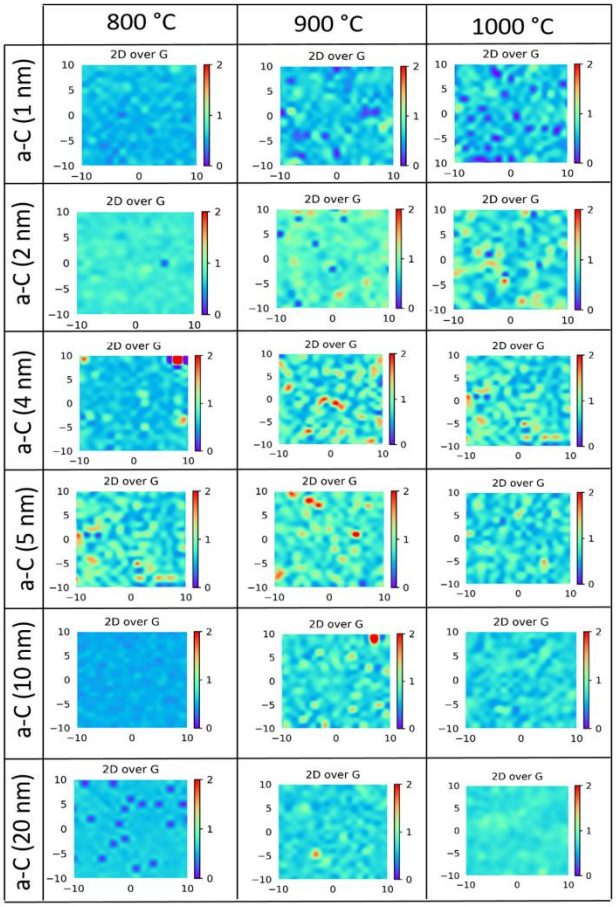

Figure 2: Raman spectroscopy maps of I_{2D}/I_G of all samples.

These maps clearly show that the as-grown film is heterogeneous, containing single to multilayer graphene sheets. The difference in the number of graphene layers is remarkable, as detailed in the Discussion section below. With an initial a-C film thickness as low as 1 nm, the I_{2D}/I_G ratio remains low (< 0.6), whatever the annealing temperature within the range 800-1 000 °C, compared to thicker a-C films. This may be because the initial carbon thickness is too thin to induce the formation of graphene layers over a large area in this temperature range, with domains exhibiting very low I_{2D}/I_G ratios. Among all growth conditions, the highest average value of I_{2D}/I_G ratio was 0.862, as can be seen on the map of the sample with an initial a-C film with a thickness of 2 nm at an annealing temperature of 900 °C. This suggests the formation of bilayer graphene. The samples a-C (4 nm - 900 °C) and a-C (5 nm - 900 °C) also had high I_{2D}/I_G ratios of 0.809 and 0.822, respectively. However, their maps look more heterogeneous than that of sample a-C (2 nm - 900 °C). Figure 3 shows the plot of average values of I_{2D}/I_G as a function of initial a-C thicknesses and synthesis temperatures. At an annealing temperature of 900 °C, we observed a progressive decrease in the I_{2D}/I_G ratio with an increase of from 2 to 20 nm in the thickness of the a-C film. This observation is consistent with that reported by Xiong et al. (Fig.4d in [36]). At 1 000 °C, the I_{2D}/I_G ratio exhibited little dependence on the initial a-C film thickness in the 2-20 nm range, whereas at 800 °C, the I_{2D}/I_G ratios were systematically lower than those at higher temperatures. Considering the same growth temperatures for each initial thickness of the a-C, 900 °C was the temperature at which the average I_{2D}/I_G ratio was higher for all initial a-C thicknesses except 20 nm. We, therefore, conclude that, in our growth conditions, the optimal temperature for high I_{2D}/I_G ratios is 900 °C.

(a)

	I_{2D}/I_G		
a-C (nm)	800 °C	900 °C	1000 °C
1	0.548	0.597	0.570
2	0.650	0.862	0.767
4	0.632	0.809	0.778
5	0.710	0.822	0.698
10	0.490	0.720	0.662
20	0.573	0.675	0.726

(b)

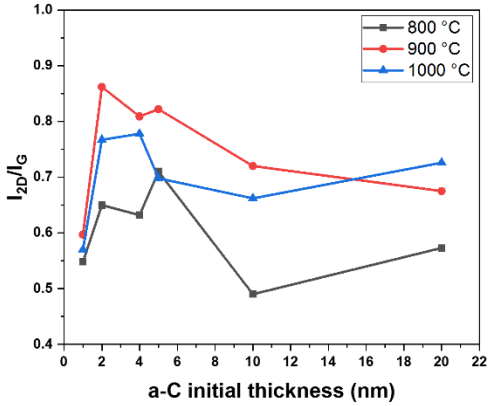

Figure 3: (a) Summary of the mean values of each I_{2D}/I_G map; (b) plot of the effect of initial a-C thickness on mean I_{2D}/I_G values as a function of growth temperature.

3.2. Density of the distribution of defects through I_D/I_G ratio mapping as a function of the initial thickness of a-C and annealing temperature

Figures 4 and 5 show the Raman maps and the average I_D/I_G ratios of all the samples for an area of 20 x 20 µm².

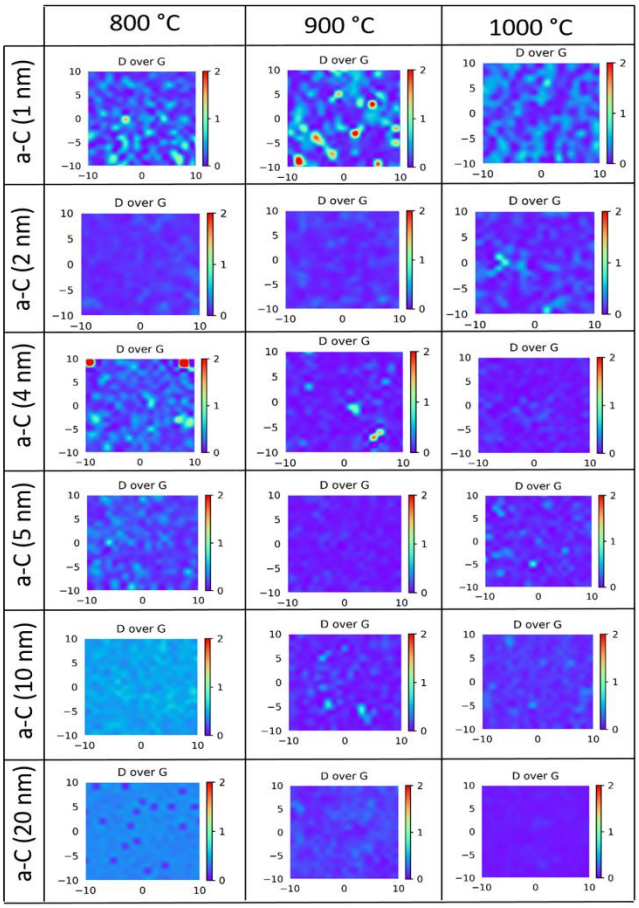

Figure 4: Raman spectroscopy maps of I_D/I_G of all the samples.

The defect density was rather homogeneous except in samples with an initial a-C thickness of 1 nm, and the homogeneity was higher at both 900 °C and 1 000 °C than at 800 °C whatever the thickness of the a-C film. The lowest average I_D/I_G ratio of 0.069 was observed for the a-C (20 nm -1 000 °C) sample. Figure 5b shows the plot of average values of the I_D/I_G ratio deduced from Figure 5a, as a function of initial a-C thickness at different synthesis temperatures. The samples grown at 900 °C and 1 000 °C had a lower defect density, with I_D/I_G ratios ranging from 0.069 to 0.163 for a-C of 2 to 20 nm. In the sample synthesized at 800 °C, the defect density was much higher, with the I_D/I_G in between 0.136 and 0.460. From these results, we conclude that a temperature of 800 °C is too low as it produces a rather high defect density in graphene films, whereas at 900 and 1 000 °C, the graphene is formed with a significantly lower defect density. This defect density is comparable with that reported with CVD synthesis[38].

(a)

a-C (nm)	I_D/I_G		
	800 °C	900 °C	1000 °C
1	0.262	0.320	0.257
2	0.248	0.131	0.152
4	0.263	0.114	0.087
5	0.212	0.081	0.125
10	0.460	0.115	0.146
20	0.353	0.163	0.069

(b)

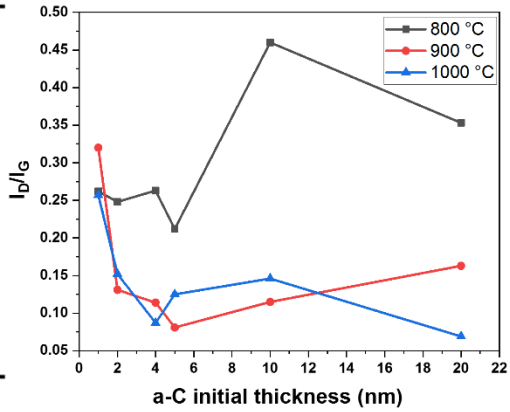

Figure 5: (a) Table summarizing the mean values of each I_D/I_G map; (b) plot of the effect of initial a-C thickness on mean I_D/I_G values as a function of growth temperature.

4. Discussion

In this section, we discuss Raman mapping statistics in order to quantify the percentage graphene layer number distribution as a function of the initial a-C film thickness and annealing temperature. In our mapping procedure, areas with an I_{2D}/I_G ratio >1.4 are considered to be representative of graphene monolayers, areas with I_{2D}/I_G ratios between 0.75 and 1.4 are considered to be representative of graphene bilayers, and areas with I_{2D}/I_G ratios below 0.75 are considered to be representative of graphene with three and more layers, as reported in the literature cited above.

Figure 6a shows the 3D plot of percentage graphene layer number distribution as a function of the initial a-C thickness at 800 °C. We observed that, at this annealing temperature, the as-grown graphene mostly had three or more layers. At a growth temperature of 900 °C (Figure 6b), graphene films contained a higher proportion of mono- and bilayers. In particular, sample a-C (2 nm) contained 89% of bilayers. At a growth temperature of 1 000 °C (Figure 6c), the

heterogeneity of the synthesized graphene was much more pronounced, mostly bilayer, and three and more layers. Therefore, we conclude that our best sample for bilayer formation is the one with an initial a-C thickness of 2 nm and the growth temperature of 900 °C when the thickness of the nickel catalyst film is fixed at 50 nm. Such an optimum low thickness of a-C to form a dominant graphene bilayer is explained on the basis of previous works related to graphene synthesis from solid carbon films in the presence of a metal catalyst. It has been already shown [24,39] that graphene growth mainly occurs during the thermal cycle by carbon dissolution and diffusion through the metal catalyst. A lower a-C film thickness of 1 nm probably does not provide enough carbon to form a homogeneous graphene layers when carbon precipitated on the Ni surface upon cooling after its dissolution during the steady-state high temperature range. Indeed, we observe that the different annealing temperatures have quite no effect on the graphene quality with such a low a-C film thickness. On the other side, an excessive initial a-C film thickness provides more carbon, but the rather high diffusion of carbon in nickel with temperature probably leads to the diffusion of carbon deep into the metal catalyst, and most of this carbon remains trapped upon cooling, limiting the quality of the graphene grown upon cooling. This may be a possible explanation of the optimum a-C film thickness of 2 nm observed with our protocol.

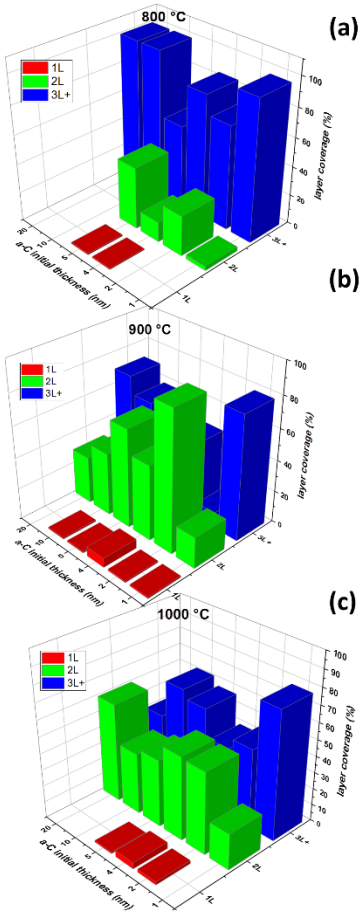

a-C (nm)	800 °C		
	1 L	2 L	3 L+
1	/	3	97
2	/	28	72
4	1	14	85
5	1	43	56
10	/	/	100
20	/	/	100

a-C (nm)	900 °C		
	1 L	2 L	3 L+
1	1	20	79
2	1	89	10
4	6	48	46
5	2	63	35
10	1	40	59
20	/	30	70

a-C (nm)	1000 °C		
	1 L	2 L	3 L+
1	/	22	78
2	2	50	48
4	4	51	41
5	1	41	58
10	/	37	63
20	/	60	40

Figure 6: Raman mapping statistics: (a) 3D plot of percentage graphene layer number distribution as a function of the initial a-C thickness (left) and the coverage percentage values (right) at 800 °C; (b) 3D plot of percentage graphene layer number distribution as a function of the initial a-C thickness (left) and the percentage distribution values (right) at 900 °C; (c) 3D plot of percentage graphene layer number distribution as a function of the initial a-C thickness (left) and the percentage distribution values (right) at 1 000 °C.

To go further in the investigation of the bilayer homogeneity related to the sample a-C (2 nm – 900 °C), we performed Raman mapping over a large area (100 x 100 µm²) with the step of 1 µm totaling 10 000 spectra. Such wide Raman mapping is rarely performed but makes it possible to obtain a more representative probed area of the graphene film.

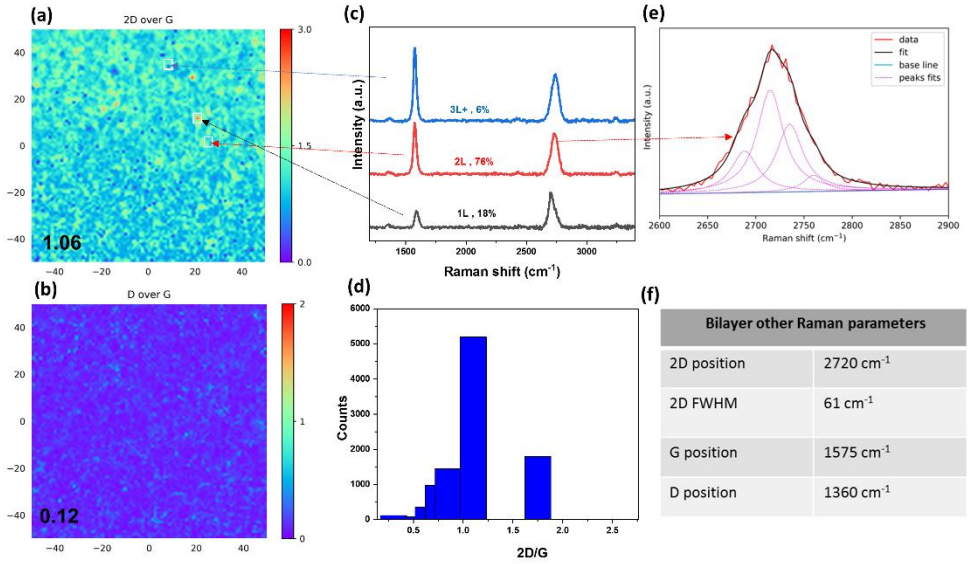

Figure 7: Raman mapping of a large 100 ×100 µm² region, of sample a-C (2 nm – 900 °C): (a) Raman mapping of I_{2D}/I_G ratio with an average value of 1.06; (b) Raman mapping of I_D/I_G ratio in a 100 ×100 µm² region with the average value of 0.12; (c) spectra of the graphene with different numbers of layers in Raman mapping of graphene on a SiO_2 substrate; (d) Statistical histogram of the Raman mapping of I_{2D}/I_G ratio showing the predominance of bilayers; (e) Fitting of the 2D band in the Raman spectrum of bilayer graphene showing an asymmetric shape and four Lorentzian peaks corresponding to AB stacking; (f) table showing the other Raman parameters of the bilayer graphene spectrum.

Figures 7a and 7b show Raman mapping of I_{2D}/I_G and I_D/I_G ratios with their average values of 1.06 and 0.12, respectively, indicating the predominant growth of bilayer and low defect density. The distribution of the number of layers was obtained by statistical analysis. We found that 18% of the 100 ×100 µm² probed area is covered by graphene monolayers, 76% by

graphene bilayers and only 6% by more than three graphene layers (Figures 7c and 7d). This result is consistent with the results of a study by Peng et al.[37] related to bilayer graphene growth using a polymer as a solid carbon source. Through Raman mapping, these authors observed 70% of bilayer coverage in an area of 100 x 100 µm². Figures 7e and 7f show the shape and Lorentzian fitting of the 2D band of the bilayer spectrum and the other Raman parameters extracted from this spectrum. The 2D band shows an asymmetric band with an FWHM around 61 cm^{-1} and can be decomposed with four Lorentzian peaks, each one with a FWHM of 30 cm^{-1}, corresponding to the AB stacking of the bilayer[35,40–42]. Our results demonstrate the possibility of synthesizing predominantly bilayer graphene with AB stacking mode from a solid carbon source using pulsed laser deposition and rapid thermal annealing, as observed by Raman over a rather large area.

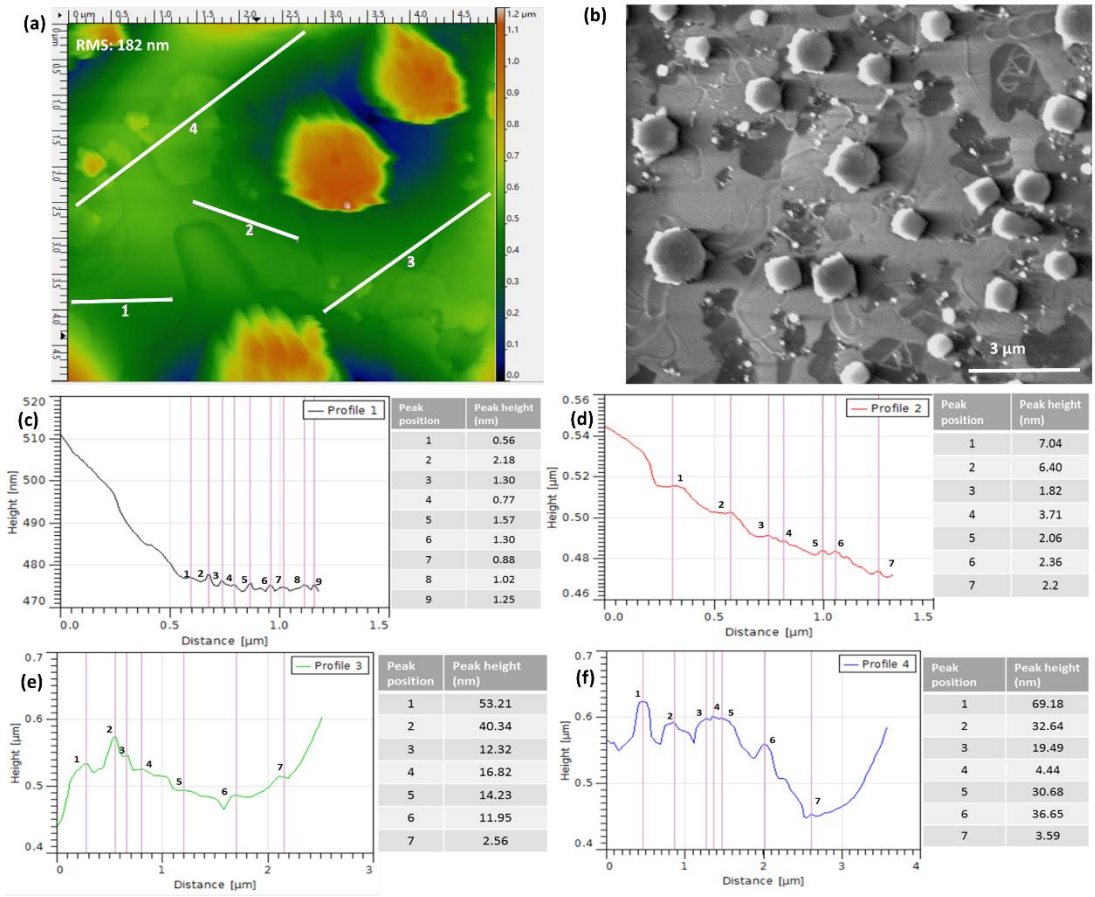

Figure 8: AFM and SEM images of sample a-C (2 nm – 900 °C): (a) AFM image showing the surface morphology with a RMS value of 182 nm; (b) SEM image showing different contrast and the nickel residual nodules; (c) AFM line profile 1 spectrum; (d) AFM line profile 2 spectrum; (e) AFM line profile 3 spectrum; (f) AFM line profile 4 spectrum. The height of all the peaks in the spectra corresponds to the thickness of the probed area.

In addition to Raman characterization, atomic force microscopy (AFM) and scanning electron microscopy (SEM) were performed to get the topological information about our best sample a-C (2 nm – 900 °C). Further XPS characterization were done in order to get the chemical composition. Additionally, since the sample was transparent after graphene synthesis, transmittance measurement was carried out for this sample.

"Figure 8a shows the surface morphology with an RMS of 182 nm observed using AFM. This image suggests a relatively rough surface with the presence of nickel clusters. The SEM image in **Figure 8b** confirms this surface morphology showing the island-shaped metallic nickel nodules. These Ni nodules have been also previously reported by others[36,43] with graphene grown in the presence of Ni catalyst, using rapid thermal annealing in the temperature range 900-1100 °C. However, we cannot exclude the presence of a residual very thin film of Ni on the rather flat areas surrounding the Ni clusters. EDX probing in such regions (not shown) confirms the presence of residual nickel. In such a way, any AFM quantification of the surface to extract the number of graphene layers should be carried out with extreme caution. Indeed, even though theoretically it is possible to measure the number of layers in AFM using the height from line profile, in practice in our case, it is hard to achieve the necessary vertical resolution with a rough surface probably covered by residual nickel. The selected lines labelled 1-2-3-4 on **Figure 8a** are typical of the surface morphology between the Ni nodules, with height quantification depicted in **Figures 8c-f**. The profile 1 gives height values between 0.56 and 2.18 nm suggesting the presence of mono and bilayer graphene, as reported in references [44,45]. The profile 2 gives height values from 1.82 to 7.04 nm suggesting the presence of bilayer to multilayer graphene. The profiles 3 and 4 give the height values rather high from 2.59 to 69.18 nm, again consistent with multilayer graphene. However, these values should take with very much care, because of the presence of nickel catalyst residual and surface roughness that may affect the thickness estimation. As mentioned before, those graphene layers certainly cover some residual Ni in the form of a very thin film on the SiO_2 substrate, thus consistent with a roughness higher than the roughness of graphene layers covering SiO_2. This is one experimental limit of the protocol used at hand, which requires in the future further investigations to obtain graphene layers without any traces of residual Ni if such a catalyst is required for the graphene growth."

In **Figure 9a**, the XPS survey spectrum of our best sample a-C (2 nm – 900 °C) shows carbon located near 284 eV, oxygen located near 533 eV and some residual of nickel. The presence of the oxygen might be due to top-surface oxidation and contamination after the a-C film

synthesis and/or during thermal annealing at 10^{-2} mbar. The nickel traces confirm what was observed by SEM and AFM. **Figure 9b** shows the C1s deconvolution into two components. The first one is centered at 284.4 eV and assigned to sp^2 hybridized C atoms in graphene. This component is the most intense and prominent in graphitic carbon indicating that most of the amorphous carbon has been transformed to graphene or graphitic carbon[46]. The other less intense component is located at 285.2 eV, corresponding to C-O bonds. **Figure 9c** shows the O1s decomposed in two components. The first component, located at 533.4 eV, and corresponds to O-C bonds. The second component, located at 531.7 eV, corresponds to O-C=O oxygen group[47–49].

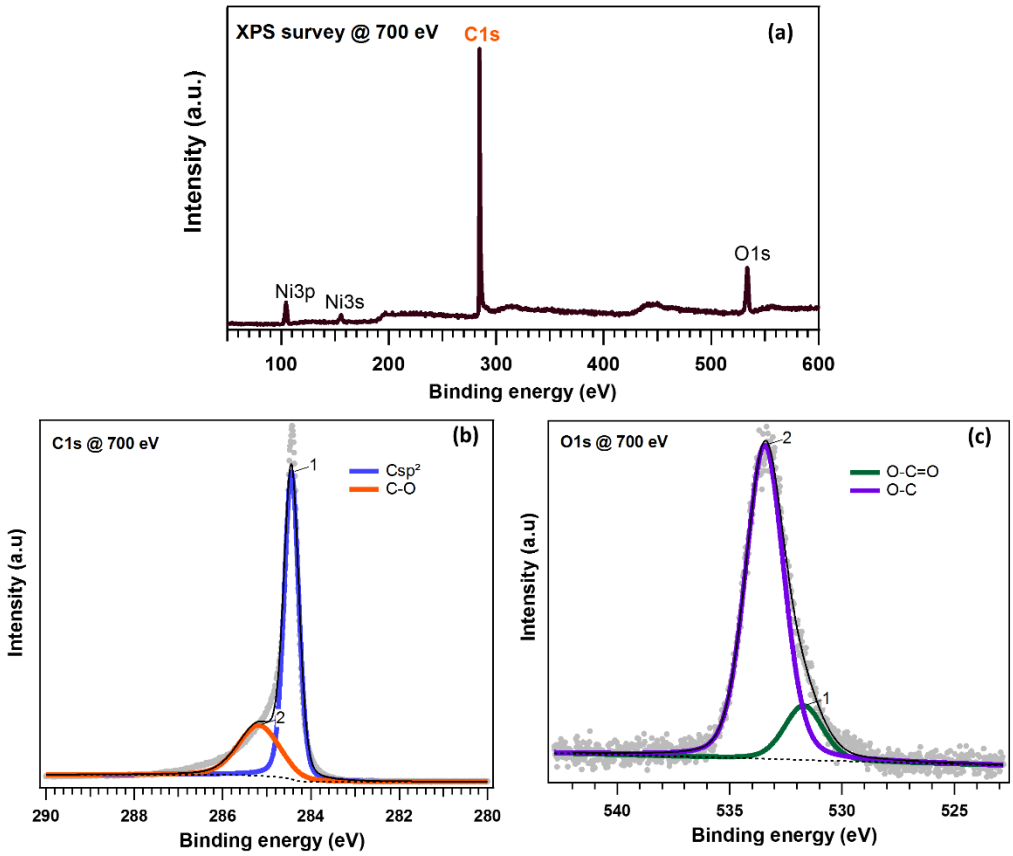

Figure 9: XPS spectra of sample a-C (2 nm – 900 °C): (a) XPS survey spectrum; (b) XPS C 1s spectrum; (c) XPS O 1s spectrum.

Since we observed nickel residual on our sample, we performed the nickel etching using 4M of $FeCl_3$ solution before the transmittance measurement. We measured the transmittance (T) of both bilayer graphene after Ni etching and the starting material before annealing (a-C (2nm)/ Ni (50)) on glass substrates for comparison (Figure 10). The transmittance values of the starting material at 550 nm is about 1.47 % (mainly due to the Ni thin film), whereas the

one for our bilayer graphene is about 87.21%. Theoretically, each graphene layer absorbs 2-3% [3] of the incident light at 550 nm, which means that the bilayer graphene transmittance value should be around 94% as reported in previous works[50,51]. Nevertheless, there is an offset between our transmittance value and the the theoretical value. However, our result is consistent with what was observed by Lee et al.[52]. They reported that the decreasing of the transmittance value can be due to the transfer method. We believe that it might a similar effect here in our case, the deviation is likely due to the remaining residual nickel nodules observed by SEM.

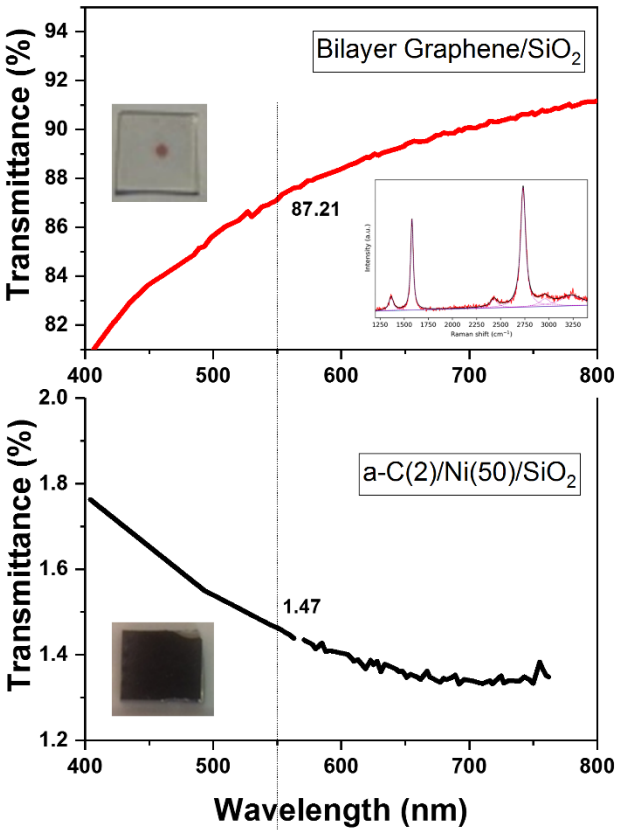

Figure 10: Transmittance curve as a function of wavelength for both: as-deposited sample (bottom) and the synthesized bilayer graphene after thermal annealing and $FeCl_3$ etching (top). The inset at the top figure shows the bilayer graphene after Ni etching.

5. Conclusion

Here, we have reported a parametric study in which we adjusted the initial thickness and growth temperature of amorphous carbon, using pulsed laser deposition and rapid thermal annealing with nickel catalyst films on a SiO_2 substrate. From the experimental findings, we deduced that the optimized process parameters to obtain a high proportion of graphene

bilayers were an initial a-C thickness of 2 nm and an annealing temperature of 900°C. A transmittance of 87% at 550 nm is observed without any transfer process from the SiO_2 substrate. Under these synthesis conditions, bilayer graphene was formed on 76% of the 100 x100 μm² probed surface, monolayer graphene on 18%, and three and more layer graphene on 6%, with a low defect density. The investigated synthesis route allows to synthetize predominantly bilayer graphene films, with a significant lower density of defect than graphene film architectures obtained by CVD without any metal catalyst. However, the residual nickel catalyst in the form of micrometer-size nodules remains a limitation to ensure a homogeneous distribution of bilayer graphene over a wide surface exempt of catalyst residues. This finding demonstrates the possibility of obtaining graphene bilayers over a large area using an alternative less frequently investigated synthesis route (compared to CVD), pulsed laser deposition combined with rapid thermal annealing. However, more work is required to investigate the synthesis of low-defect graphene films from a solid carbon source, without any use of metal catalyst.

Acknowledgments

This work was conducted with the financial support of the Future Program Lyon Saint-Etienne (PALSE) in the framework of the LABEX MANUTECH-SISE (ANR-10-LABX-0075) from the University of Lyon (ANR-11-IDEX-0007), under the *Investissements d'Avenir* program managed by the French National Research Agency (French acronym ANR).

References

[1] A.K. Geim, K.S. Novoselov, The rise of graphene, Nat. Mater. 6 (2007) 183–191. doi:10.1038/nmat1849.
[2] K.S. Novoselov, A.K. Geim, S.V. Morozov, D. Jiang, Y. Zhang, S.V. Dubonos, I.V. Grigorieva, A.A. Firsov, Electric Field Effect in Atomically Thin Carbon Films, Science. 306 (2004) 666–669. doi:10.1126/science.1102896.
[3] R.R. Nair, P. Blake, A.N. Grigorenko, K.S. Novoselov, T.J. Booth, T. Stauber, N.M.R. Peres, A.K. Geim, Fine Structure Constant Defines Visual Transparency of Graphene, Science. 320 (2008) 1308–1308. doi:10.1126/science.1156965.
[4] Y.D. Kim, M.-H. Bae, J.-T. Seo, Y.S. Kim, H. Kim, J.H. Lee, J.R. Ahn, S.W. Lee, S.-H. Chun, Y.D. Park, Focused-Laser-Enabled p–n Junctions in Graphene Field-Effect Transistors, ACS Nano. 7 (2013) 5850–5857. doi:10.1021/nn402354j.
[5] F. Bonaccorso, Z. Sun, T. Hasan, A.C. Ferrari, Graphene photonics and optoelectronics, Nat. Photonics. 4 (2010) 611–622. doi:10.1038/nphoton.2010.186.

[6] K.V. Emtsev, A. Bostwick, K. Horn, J. Jobst, G.L. Kellogg, L. Ley, J.L. McChesney, T. Ohta, S.A. Reshanov, J. Röhrl, E. Rotenberg, A.K. Schmid, D. Waldmann, H.B. Weber, T. Seyller, Towards wafer-size graphene layers by atmospheric pressure graphitization of silicon carbide, Nat. Mater. 8 (2009) 203–207. doi:10.1038/nmat2382.
[7] X. Li, C.W. Magnuson, A. Venugopal, J. An, J.W. Suk, B. Han, M. Borysiak, W. Cai, A. Velamakanni, Y. Zhu, L. Fu, E.M. Vogel, E. Voelkl, L. Colombo, R.S. Ruoff, Graphene Films with Large Domain Size by a Two-Step Chemical Vapor Deposition Process, Nano Lett. 10 (2010) 4328–4334. doi:10.1021/nl101629g.
[8] R. Hawaldar, P. Merino, M.R. Correia, I. Bdikin, J. Grácio, J. Méndez, J.A. Martín-Gago, M.K. Singh, Large-area high-throughput synthesis of monolayer graphene sheet by Hot Filament Thermal Chemical Vapor Deposition, Sci. Rep. 2 (2012) 682. doi:10.1038/srep00682.
[9] Y. Bleu, F. Bourquard, T. Tite, A.-S. Loir, C. Maddi, C. Donnet, F. Garrelie, Review of Graphene Growth From a Solid Carbon Source by Pulsed Laser Deposition (PLD), Front. Chem. 6 (2018). doi:10.3389/fchem.2018.00572.
[10] S. Pei, H.-M. Cheng, The reduction of graphene oxide, Carbon. 50 (2012) 3210–3228. doi:10.1016/j.carbon.2011.11.010.
[11] H.-U. Krebs, M. Weisheit, J. Faupel, E. Süske, T. Scharf, C. Fuhse, M. Störmer, K. Sturm, M. Seibt, H. Kijewski, D. Nelke, E. Panchenko, M. Buback, Pulsed Laser Deposition (PLD) -- A Versatile Thin Film Technique, in: Adv. Solid State Phys., Springer, Berlin, Heidelberg, n.d.: pp. 505–518. doi:10.1007/978-3-540-44838-9_36.
[12] A. Sikora, F. Garrelie, C. Donnet, A.S. Loir, J. Fontaine, J.C. Sanchez-Lopez, T.C. Rojas, Structure of diamondlike carbon films deposited by femtosecond and nanosecond pulsed laser ablation, J. Appl. Phys. 108 (2010) 113516. doi:10.1063/1.3510483.
[13] Q. Liu, Y. Gong, T. Wang, W.-L. Chan, J. Wu, Metal-catalyst-free and controllable growth of high-quality monolayer and AB-stacked bilayer graphene on silicon dioxide, Carbon. 96 (2016) 203–211. doi:10.1016/j.carbon.2015.09.075.
[14] A.N. Barbosa, F. Ptak, C.D. Mendoza, M.E.H. Maia da Costa, F.L. Freire Jr, Direct synthesis of bilayer graphene on silicon dioxide substrates, Diam. Relat. Mater. 95 (2019) 71–76. doi:10.1016/j.diamond.2019.04.006.
[15] A. Reina, S. Thiele, X. Jia, S. Bhaviripudi, M.S. Dresselhaus, J.A. Schaefer, J. Kong, Growth of large-area single- and Bi-layer graphene by controlled carbon precipitation on polycrystalline Ni surfaces, Nano Res. 2 (2009) 509–516. doi:10.1007/s12274-009-9059-y.
[16] A. Delamoreanu, C. Rabot, C. Vallee, A. Zenasni, Wafer scale catalytic growth of graphene on nickel by solid carbon source, Carbon. 66 (2014) 48–56. doi:10.1016/j.carbon.2013.08.037.
[17] A.E.M. Abd Elhamid, M.A. Hafez, A.M. Aboulfotouh, I.M. Azzouz, Study of graphene growth on copper foil by pulsed laser deposition at reduced temperature, J. Appl. Phys. 121 (2017) 025303. doi:10.1063/1.4973736.
[18] U. Narula, C.M. Tan, C.S. Lai, Copper induced synthesis of graphene using amorphous carbon, Microelectron. Reliab. 61 (2016) 87–90. doi:10.1016/j.microrel.2016.01.005.
[19] P. Tyagi, Z.R. Robinson, A. Munson, C.W. Magnuson, S. Chen, J.D. McNeilan, R.L. Moore, R.D. Piner, R.S. Ruoff, C.A. Ventrice, Characterization of graphene films grown on CuNi foil substrates, Surf. Sci. 634 (2015) 16–24. doi:10.1016/j.susc.2014.11.019.
[20] C.M. Orofeo, H. Ago, B. Hu, M. Tsuji, Synthesis of large area, homogeneous, single layer graphene films by annealing amorphous carbon on Co and Ni, Nano Res. 4 (2011) 531–540. doi:10.1007/s12274-011-0109-x.

[21] T. Tite, C. Donnet, A.-S. Loir, S. Reynaud, J.-Y. Michalon, F. Vocanson, F. Garrelie, Graphene-based textured surface by pulsed laser deposition as a robust platform for surface enhanced Raman scattering applications, Appl. Phys. Lett. 104 (2014) 041912.
[22] P. Fortgang, T. Tite, V. Barnier, N. Zehani, C. Maddi, F. Lagarde, A.-S. Loir, N. Jaffrezic-Renault, C. Donnet, F. Garrelie, C. Chaix, Robust Electrografting on Self-Organized 3D Graphene Electrodes, ACS Appl. Mater. Interfaces. 8 (2016) 1424–1433. doi:10.1021/acsami.5b10647.
[23] C. Maddi, F. Bourquard, V. Barnier, J. Avila, M.-C. Asensio, T. Tite, C. Donnet, F. Garrelie, Nano-Architecture of nitrogen-doped graphene films synthesized from a solid CN source, Sci. Rep. 8 (2018). doi:10.1038/s41598-018-21639-9.
[24] A.T.T. Koh, Y.M. Foong, D.H.C. Chua, Comparison of the mechanism of low defect few-layer graphene fabricated on different metals by pulsed laser deposition, Diam. Relat. Mater. 25 (2012) 98–102. doi:10.1016/j.diamond.2012.02.014.
[25] H. Zhang, P.X. Feng, Fabrication and characterization of few-layer graphene, Carbon. 48 (2010) 359–364. doi:10.1016/j.carbon.2009.09.037.
[26] F. Bourquard, Y. Bleu, A.-S. Loir, B. Caja-Munoz, J. Avila, M.-C. Asensio, G. Raimondi, M. Shokouhi, I. Rassas, C. Farre, C. Chaix, V. Barnier, N. Jaffrezic-Renault, F. Garrelie, C. Donnet, Electroanalytical Performance of Nitrogen-Doped Graphene Films Processed in One Step by Pulsed Laser Deposition Directly Coupled with Thermal Annealing, Materials. 12 (2019) 666. doi:10.3390/ma12040666.
[27] C.-M. Seah, S.-P. Chai, A.R. Mohamed, Mechanisms of graphene growth by chemical vapour deposition on transition metals, Carbon. 70 (2014) 1–21. doi:10.1016/j.carbon.2013.12.073.
[28] Y. Zhang, L. Zhang, C. Zhou, Review of Chemical Vapor Deposition of Graphene and Related Applications, Acc. Chem. Res. 46 (2013) 2329–2339. doi:10.1021/ar300203n.
[29] X. Li, W. Cai, L. Colombo, R.S. Ruoff, Evolution of Graphene Growth on Ni and Cu by Carbon Isotope Labeling, Nano Lett. 9 (2009) 4268–4272. doi:10.1021/nl902515k.
[30] S. Pang, Y. Hernandez, X. Feng, K. Müllen, Graphene as Transparent Electrode Material for Organic Electronics, Adv. Mater. 23 (2011) 2779–2795. doi:10.1002/adma.201100304.
[31] R.S. Weatherup, B.C. Bayer, R. Blume, C. Baehtz, P.R. Kidambi, M. Fouquet, C.T. Wirth, R. Schlögl, S. Hofmann, On the Mechanisms of Ni-Catalysed Graphene Chemical Vapour Deposition, ChemPhysChem. 13 (2012) 2544–2549. doi:10.1002/cphc.201101020.
[32] A.C. Ferrari, J.C. Meyer, V. Scardaci, C. Casiraghi, M. Lazzeri, F. Mauri, S. Piscanec, D. Jiang, K.S. Novoselov, S. Roth, A.K. Geim, Raman Spectrum of Graphene and Graphene Layers, Phys. Rev. Lett. 97 (2006) 187401. doi:10.1103/PhysRevLett.97.187401.
[33] D. Graf, F. Molitor, K. Ensslin, C. Stampfer, A. Jungen, C. Hierold, L. Wirtz, Raman mapping of a single-layer to double-layer graphene transition, Eur. Phys. J. Spec. Top. 148 (2007) 171–176. doi:10.1140/epjst/e2007-00237-1.
[34] L.M. Malard, M.A. Pimenta, G. Dresselhaus, M.S. Dresselhaus, Raman spectroscopy in graphene, Phys. Rep. 473 (2009) 51–87. doi:10.1016/j.physrep.2009.02.003.
[35] Y. Gong, X. Zhang, G. Liu, L. Wu, X. Geng, M. Long, X. Cao, Y. Guo, W. Li, J. Xu, M. Sun, L. Lu, L. Liu, Layer-Controlled and Wafer-Scale Synthesis of Uniform and High-Quality Graphene Films on a Polycrystalline Nickel Catalyst, Adv. Funct. Mater. 22 (2012) 3153–3159. doi:10.1002/adfm.201200388.
[36] W. Xiong, Y.S. Zhou, L.J. Jiang, A. Sarkar, M. Mahjouri- Samani, Z.Q. Xie, Y. Gao, N.J. Ianno, L. Jiang, Y.F. Lu, Single-Step Formation of Graphene on Dielectric Surfaces, Adv. Mater. 25 (2013) 630–634. doi:10.1002/adma.201202840.

[37] Z. Peng, Z. Yan, Z. Sun, J.M. Tour, Direct Growth of Bilayer Graphene on SiO2 Substrates by Carbon Diffusion through Nickel, ACS Nano. 5 (2011) 8241–8247. doi:10.1021/nn202923y.
[38] A. Umair, H. Raza, Controlled synthesis of bilayer graphene on nickel, Nanoscale Res. Lett. 7 (2012). doi:10.1186/1556-276X-7-437.
[39] R.S. Weatherup, C. Baehtz, B. Dlubak, B.C. Bayer, P.R. Kidambi, R. Blume, R. Schloegl, S. Hofmann, Introducing Carbon Diffusion Barriers for Uniform, High-Quality Graphene Growth from Solid Sources, Nano Lett. 13 (2013) 4624–4631. doi:10.1021/nl401601x.
[40] M.J. Madito, A. Bello, J.K. Dangbegnon, C.J. Oliphant, W.A. Jordaan, T.M. Masikhwa, D.Y. Momodu, N. Manyala, Raman analysis of bilayer graphene film prepared on commercial Cu(0.5 at% Ni) foil, J. Raman Spectrosc. 47 (2016) 553–559. doi:10.1002/jrs.4848.
[41] N. Yang, K. Choi, J. Robertson, H.G. Park, Layer-selective synthesis of bilayer graphene via chemical vapor deposition, 2D Mater. 4 (2017) 035023. doi:10.1088/2053-1583/aa805d.
[42] W. Fang, A.L. Hsu, R. Caudillo, Y. Song, A.G. Birdwell, E. Zakar, M. Kalbac, M. Dubey, T. Palacios, M.S. Dresselhaus, P.T. Araujo, J. Kong, Rapid Identification of Stacking Orientation in Isotopically Labeled Chemical-Vapor Grown Bilayer Graphene by Raman Spectroscopy, Nano Lett. 13 (2013) 1541–1548. doi:10.1021/nl304706j.
[43] K. Banno, M. Mizuno, K. Fujita, T. Kubo, M. Miyoshi, T. Egawa, T. Soga, Transfer-free graphene synthesis on insulating substrates via agglomeration phenomena of catalytic nickel films, Appl. Phys. Lett. 103 (2013) 082112. doi:10.1063/1.4818342.
[44] Y. Yao, L. Ren, S. Gao, S. Li, Histogram method for reliable thickness measurements of graphene films using atomic force microscopy (AFM), J. Mater. Sci. Technol. 33 (2017) 815–820. doi:10.1016/j.jmst.2016.07.020.
[45] E.A. Obraztsova, A.V. Osadchy, E.D. Obraztsova, S. Lefrant, I.V. Yaminsky, Statistical analysis of atomic force microscopy and Raman spectroscopy data for estimation of graphene layer numbers, Phys. Status Solidi B. 245 (2008) 2055–2059. doi:10.1002/pssb.200879657.
[46] R. Blume, D. Rosenthal, J.-P. Tessonnier, H. Li, A. Knop- Gericke, R. Schlögl, Characterizing Graphitic Carbon with X-ray Photoelectron Spectroscopy: A Step-by-Step Approach, ChemCatChem. 7 (2015) 2871–2881. doi:10.1002/cctc.201500344.
[47] Y. Wang, Y. Shao, D.W. Matson, J. Li, Y. Lin, Nitrogen-Doped Graphene and Its Application in Electrochemical Biosensing, ACS Nano. 4 (2010) 1790–1798. doi:10.1021/nn100315s.
[48] C. Malitesta, I. Losito, L. Sabbatini, P.G. Zambonin, New findings on polypyrrole chemical structure by XPS coupled to chemical derivatization labelling, J. Electron Spectrosc. Relat. Phenom. 76 (1995) 629–634. doi:10.1016/0368-2048(95)02438-7.
[49] A. Ganguly, S. Sharma, P. Papakonstantinou, J. Hamilton, Probing the Thermal Deoxygenation of Graphene Oxide Using High-Resolution In Situ X-ray-Based Spectroscopies, J. Phys. Chem. C. 115 (2011) 17009–17019. doi:10.1021/jp203741y.
[50] Z. Sun, Z. Yan, J. Yao, E. Beitler, Y. Zhu, J.M. Tour, Growth of graphene from solid carbon sources, Nature. 468 (2010) 549–552. doi:10.1038/nature09579.
[51] Q. Liu, Y. Gong, J.S. Wilt, R. Sakidja, J. Wu, Synchronous growth of AB-stacked bilayer graphene on Cu by simply controlling hydrogen pressure in CVD process, Carbon. 93 (2015) 199–206. doi:10.1016/j.carbon.2015.05.063.
[52] S. Lee, K. Lee, C.-H. Liu, Z. Zhong, Homogeneous bilayer graphene film based flexible transparent conductor, Nanoscale. 4 (2012) 639–644. doi:10.1039/C1NR11574J.